Geochemical insights into the internal dynamics of debris avalanches. A case study: The Socompa avalanche, Chile

Régis Doucelance, Karim Kelfoun, Philippe Labazuy, Chantal Bosq

AGU PUBLICATIONS

Geochemistry, Geophysics, Geosystems

RESEARCH ARTICLE
10.1002/2014GC005235

Key Points:
- We characterize the geochemical heterogeneity of the Socompa avalanche deposit
- We present Sr-Nd isotope ratios for matrices and rock fragments from the deposit
- The isotopic heterogeneity of the deposits increases from source to front

Supporting Information:
- Data table
- Additional figures
- Readme

Correspondence to:
R. Doucelance,
r.doucelance@opgc.univ-bpclermont.fr

Citation:
Doucelance, R., K. Kelfoun, P. Labazuy, and C. Bosq (2014), Geochemical insights into the internal dynamics of debris avalanches. A case study: The Socompa avalanche, Chile, *Geochem. Geophys. Geosyst.*, *15*, 2282–2300, doi:10.1002/2014GC005235.

Received 8 JAN 2014
Accepted 18 APR 2014
Accepted article online 23 APR 2014
Published online 6 JUN 2014

Geochemical insights into the internal dynamics of debris avalanches. A case study: The Socompa avalanche, Chile

Régis Doucelance[1,2,3], Karim Kelfoun[1,2,3], Philippe Labazuy[1,2,3], and Chantal Bosq[1,2,3]

[1]Laboratoire Magmas et Volcans, Université Blaise Pascal, Clermont-Ferrand, France, [2]CNRS, UMR 6524, LMV, Clermont-Ferrand, France, [3]IRD, R 163, LMV, Clermont-Ferrand, France

Abstract One way to infer the internal dynamics of debris avalanches is to characterize the heterogeneity of their deposits. Here we present high-precision Sr-Nd isotope compositions, plus major and trace element concentrations, of matrix samples and rock fragments from the Socompa debris-avalanche deposit (Chile). The Socompa blocks are easily identifiable in the field, but distinguishing substrate debris from disaggregated material formed at the volcano is difficult to do with only field criteria. Combining isotope data with field observations can help with this. Measured Sr and Nd isotope ratios show significant variations, defining a binary mixing array where matrix and rock deposits overlap. This testifies to the mixing of crushed rocks during collapse and/or movement. Assimilation of Socompa basement appears to be variable; overall, it is far lower than was previously proposed. Comparison between matrix and block samples in contact, over the whole surface area of the deposit, shows that the isotopic heterogeneity increases from source to front. Close to the Socompa, matrices are resulting from simple crushing of adjacent rocks. At the front, rock samples with distinct compositions are found in a close relationship with matrices that result either from mixing of these (or some of these) rocks or from crushing of basement material. Between the source and the front, the efficient mixing of Socompa rocks (and basement rocks) generates matrices with isotopic compositions distinct from those of the blocks they are in contact with. We interpret these results as being due to more efficient vertical mixing during the avalanche emplacement.

1. Introduction

Volcanic debris avalanches are hazardous phenomena resulting from the gravitational collapse of volcanic edifice flanks [*Voight et al.*, 1981; *Ui*, 1983; *Crandell et al.*, 1984; *Siebert*, 1984]. They comprise large volumes of crushed rock (millions of m^3 to tens of km^3).

A major characteristic of large debris avalanches is their very long runout: they often reach some tens of kilometres for a thickness of tens to hundreds of meters, with inferred velocities of up to 100 m s^{-1}. The ability of avalanches to travel large distances in a fluid-like manner is not well understood, and a number of possible friction reduction mechanisms have been proposed [e.g., *Davies and McSaveney*, 1999; *Legros*, 2002; *Collins and Melosh*, 2003, and references therein].

To better understand the emplacement of large debris avalanches and to determine what mechanisms are involved in their long runouts, we must answer the following key questions. Do the avalanches behave as a solid that slides on its base, or do they behave globally as a fluid? In the latter case, where are the fluid parts located? Does the fluidity change in time and space? How, where, and when do the rocks of the long runout avalanches break and mix? This last point can provide insight into the movements that affect the broken rocks during emplacement. It also allows the energy needed for, and released by, rock breaking to be estimated. Understanding these different aspects is of particular interest for natural hazard management [*Stoopes and Sheridan*, 1992; *Capra et al.*, 2002].

Numerical modeling and laboratory experiments can be used to answer the above questions. Some models simulate the set of particles as a continuous flow [e.g., *Mangeney et al.*, 2000; *Iverson and Denlinger*, 2001; *Kelfoun and Druitt*, 2005]. Thus, they allow the global mechanical behavior of the natural flows to be determined, and their emplacement history reconstructed. They cannot, however, simulate the complexity of particle interactions. Discrete element models simulate each particle of the destabilization and of the flow [e.g., *Campbell*, 1989; *Morgan and McGovern*, 2005; *Mollon et al.*, 2012]. They show that the initial distribution of rocks is globally conserved along the avalanche and that particles mix over distances of a few particle

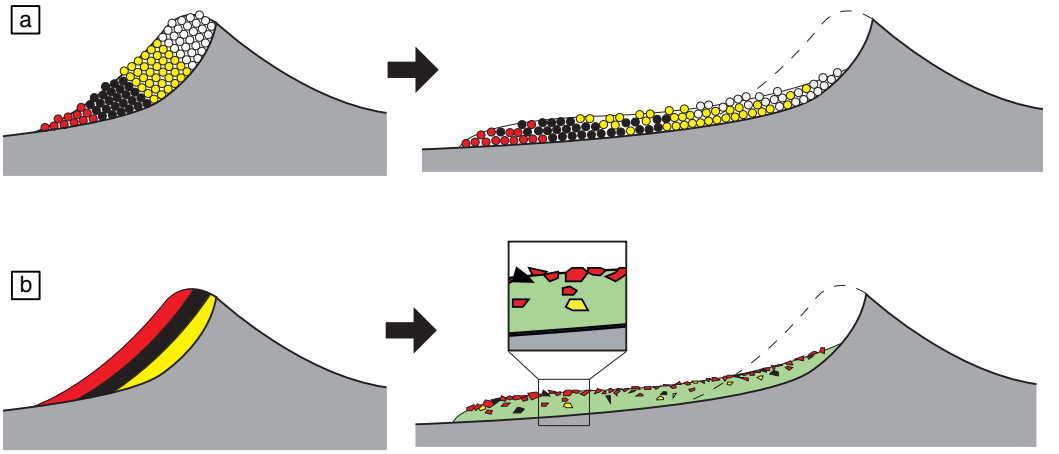

Figure 1. Schematic cartoons showing the different mechanisms of debris-avalanche internal dynamics, as seen by (a) laboratory experiments and discrete element modeling and (b) field observations. Models in Figure 1a simulate the distribution of particles (here represented by colored circles) after collapse. Field works in Figure 1b show that initially coherent rocks are crushed and then form the matrix of the avalanche (in green). None of these approaches are able to explain where, when, and how the formation of the matrix occurs.

diameters (Figure 1). Laboratory experiments based on granular mass spreading [*Shea and van Wyk de Vries*, 2008] lead to similar lithology distributions than discrete element simulations. They also produce morphologies and structures that resemble those observed in the field. The maximum number of particles that can be modeled limits both approaches, and the finest particle is equivalent to blocks larger than several meters in the field.

Field observations suggest that the very high fluidity of natural flows and the long runouts of debris avalanches are related to the presence of abundant, fine particles. The latter ones are resulting from the crushing of transported rocks from the volcanic edifice, and their whole set define the matrix of the avalanche (Figure 1) that can represent a large proportion of the deposits ($\geq$50%) [cf., *Crandell*, 1989; *van Wyk de Vries et al*., 2001]. Understanding the matrix formation and studying its behavior are thus of great importance. However, up to date neither numerical nor laboratory models are simulating rock breaking, matrix formation, and mixing within the matrix. Furthermore, constraints brought to the matrix formation by field observations are limited due to difficulties in deciphering the origin of crushed rocks. Hence, we need a new tool to study how the rock breaks and mixes in debris avalanches in order to better understand their dynamics.

In this study, we focus on the Socompa debris-avalanche deposits in Chile. Their location in the Atacama desert, which has one of the most arid climates on the Earth's surface, has led to very good preservation of their morphology, structure, and lithology [*Ramirez*, 1988] and also guarantees that their chemical composition has barely been modified (if at all) by low-temperature/supergene alteration. The Socompa avalanche shares the same morphological and structural characteristics as other debris avalanches worldwide (notably Aucanquilcha, Lastarria, and Llullaillaco debris avalanches) [cf., *Richards and Villeneuve*, 2001; *Shea and van Wyk de Vries*, 2008]. Thus, it constitutes one of the best places to study debris-avalanche deposits.

We present geochemical analyses (major and trace element concentrations, as well as isotope ratios) of the main constituents of the deposits: (1) rock fragments (or blocks) transported on the deposit surface, which are inferred to be derived directly from the volcanic edifice affected by gravitational collapse and (2) matrix samples, resulting from the crushing of transported rocks from the volcanic edifice, possibly incorporating rocks on which the avalanche flowed. We combine high-precision $^{87}Sr/^{86}Sr$ and $^{143}Nd/^{144}Nd$ source tracers with differentiation markers (major and trace elements). Using these, we are able to infer the degree of heterogeneity of the Socompa deposits and thus the internal dynamics and the spatial scale of mixing in the deposits. We are also interested in whether the matrix results solely from the crushing and mixing of the volcanic rocks that collapsed, or whether rocks covered by the avalanche also participate, and if so, to what extent.

We will show that relationships between blocks and matrices in contact are related to the sector of the avalanche where they have been collected, and to the history of their emplacement. Thus, at large scale, the level of heterogeneity of deposits is increasing with the distance from the Socompa edifice summit. Mixing

involving rocks on which the avalanche emplaced, however, seems to be limited. In any case, such a contribution is variable.

2. Geological Setting and Sampling Details

The Socompa debris-avalanche deposits (Figure 2) were initially interpreted as resulting from a large eruption and pyroclastic flow [*Deruelle*, 1978] because of their high percentage of pumice clasts. Subsequently, *Francis et al*. [1985] recognized them as the collapse of a 70° sector of the northwestern flank of Socompa volcano.

The Socompa debris avalanche took place about 7200 yr BP (^{14}C estimate) [see *Wadge et al*., 1995]. The deposit covers an area of 490 km^2 (35 km length) and has a volume of at least 15 km^3. Four main zones can be distinguished based on the morphology of deposits: (1) the proximal zone; (2) the distal zone that corresponds to large extensional areas in the backward movement sector where matrix crops out; (3) the median escarpment that delimits the front of the backward movement; and (4) the frontal zones and levees (Figure 2).

Wadge et al. [1995] and *van Wyk de Vries et al*. [2001] inferred that the Socompa volcano basement rocks have played a role in the avalanche. Here the term basement does not refer to crystalline rocks, but to surface rocks covered by the avalanche. The latter ones include gravels, pyroclastic flow deposits, and lava flows, making up the Quebrada Salin Beds formation, intercalated toward the top with sheets of the Arenosa and Tucucaro ignimbrites [*Wadge et al*., 1995; *van Wyk de Vries et al*., 2001]. The uppermost part of the basement crops out around and within the debris-avalanche deposits and is well preserved at the locality of La Flexura (Figure 2). *Wadge et al*. [1995] calculated a volumetric contribution of basement material to the deposits of ~60%. Using new field measurements, facilitated by roads accessing water-drilling platforms, *van Wyk de Vries et al*. [2001] revised these proportions and proposed that about 80% of the Socompa avalanche deposits is La Flexura-like basement material.

Numerical modeling of the Socompa avalanche has successfully reproduced both the morphology and measured thickness of deposits [*Kelfoun and Druitt*, 2005]. The conclusions drawn from the model have been confirmed by detailed analysis of the avalanche deposit morphology and structures and by the reconstruction of surface displacements [*Kelfoun et al*., 2008]. This allows us to place important constraints on the mass movement and timing of the avalanche emplacement, which we used to select sample locations and to provide a framework for interpreting our results. The deposit morphologies and structures are explained by complex movements of the avalanche due to the shape of the Monturaqui basin, the topographic depression into which it was emplaced. Initially, the avalanche resulting from the collapse of Socompa travelled northwestward, across the basin. It then slowed down on reaching the north side of the basin, where the frontal part of the deposits stopped and formed a marginal levee. The rest of the avalanche thickened before moving about 15 km back toward the center of the depression, with the front of the backward movement forming the median escarpment, one of the main features of the Socompa debris-avalanche deposit [*Francis et al*., 1985]. According to the numerical simulation of *Kelfoun and Druitt* [2005], the whole debris-avalanche deposit was emplaced in about 12 min.

In order to understand the relationship between the matrix and the rocks from the Socompa debris-avalanche deposits and the associated dynamical aspects, we focused on key zones that have already been studied [*Francis et al*., 1985; *Wadge et al*., 1995; *van Wyk de Vries et al*., 2001; *Kelfoun et al*., 2008]. We collected deposit samples as well as rocks representative of the basement (La Flexura inlier and tertiary volcanism) and local magnesium-rich and calcium-rich unconsolidated sediments. Avalanche deposit samples were of two distinct types: either rocks or matrix (crushed) samples. We also collected samples from Torevas (located at the beginning of the proximal zone; cf., Figure 2), which are large, coherent blocks that collapsed but were not dismantled [*Wadge et al*., 1995]. The absence of deposits on their tops suggests that they slid into place during or after the main debris avalanche passed downslope.

Matrices were generally fine grained, but sometimes contained larger inclusions (cm to few cm, or even greater) with no size continuity through to the smaller particles. Hence, we did not consider the elements greater than a few millimetres in size as being part of the matrix samples. Instead, they were categorized as clasts and considered as distinct samples. We chose the value of 1–2 mm as the matrix/clast division in

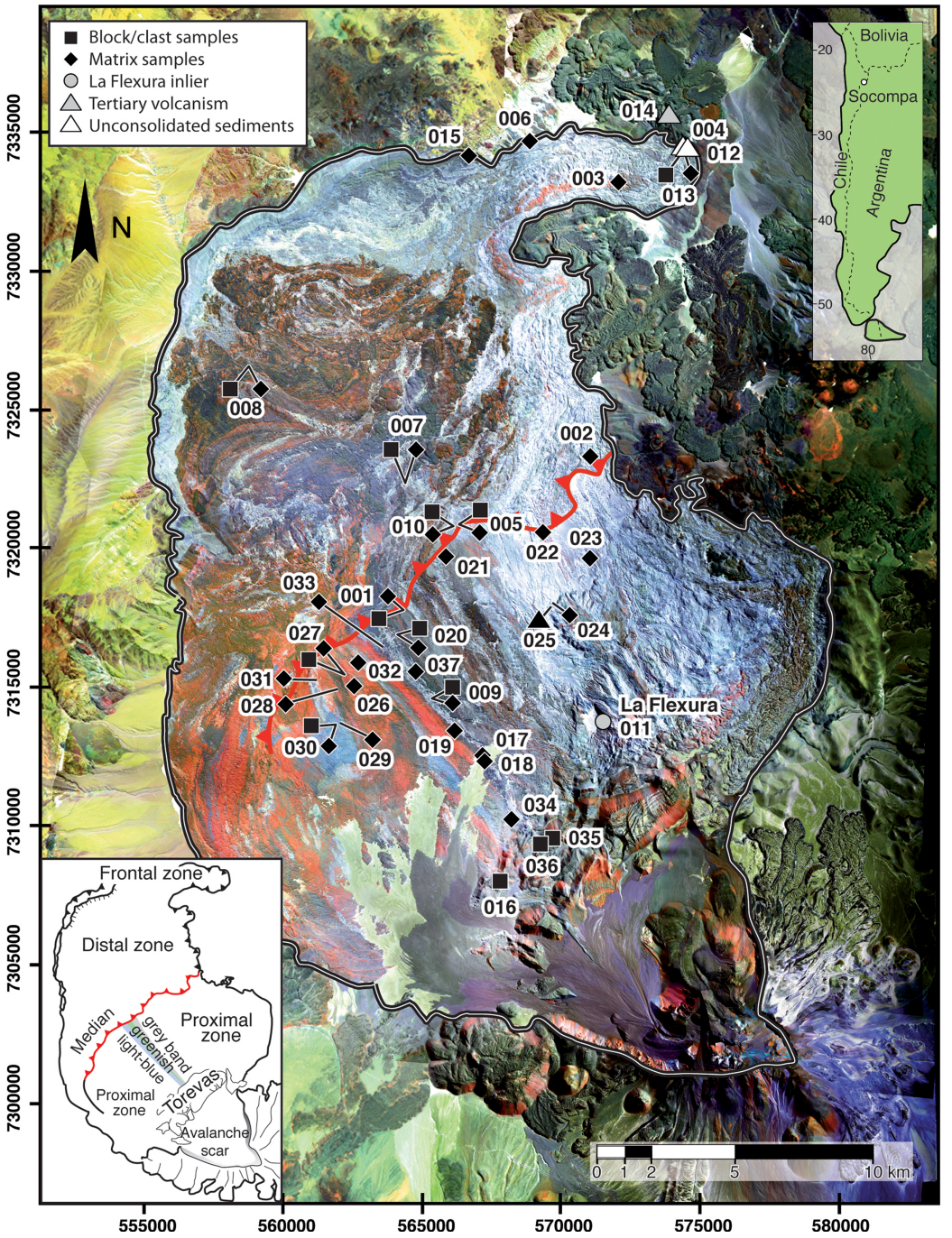

Figure 2. Geographical map of the Socompa debris-avalanche deposits with sample locations and outcrop numbers (modified from *Kelfoun et al.* [2008]). Colors are obtained by combining bands 7, 4, and 1 of Landsat image. The thick, red line corresponds to the median escarpment; inset at the bottom left shows the four main zones that can be distinguished based on the morphology of deposits: (1) the proximal zone; (2) the distal zone that corresponds to the large extensional areas in the backward movement sector; (3) the median escarpment that delimits the front of the backward movement; and (4) the frontal zones and levees. UTM coordinates: WGS84, zone 19S.

order to make it possible to distinguish visually between clasts and matrices in the field and thus facilitate sampling of the avalanche deposits. Where possible, we collected matrix and representative rock samples that were in contact.

Samples are labelled as follows: Outcrop number—R or M for Rock or Matrix—sample number. For instance, 5-M2 is the second matrix sample at outcrop 5. Their locations are shown in Figure 2, where only the outcrop

numbers have been marked so as to make it easier to read (see also supporting information Figure S1). Rocks refer to either blocks or clasts. Their distinction is not related to their composition or their size, but it notifies where they were sampled: at the surface of the deposits for blocks, or within matrices for clasts.

3. Analytical Procedures and Methodology

3.1. Major and Trace Elements and Sr-Nd Isotopic Ratios

Hundred to two hundred grams of each sample were reduced into chips in a jaw crusher before being powdered in an agate swing mill. Fine crushing was performed in three steps: (1) the first crushing run was conducted to precontaminate the agate mill; (2) the second run was used for major and trace element determinations; and (3) the third one for Sr-Nd isotope analyses.

Both major and trace element (Ba and Sr) contents were determined at the Magmas and Volcans Laboratory (LMV) using Inductively Coupled Plasma-Atomic Emission Spectrometry (ICP-AES, Ultima-C instrument) after alkaline melting with lithium metaborate/tetraborate and nitric acid dissolution (100 mg of sample). BHVO-1 standard measurements along with Socompa samples, as well as duplicate measurements of the lowest-SiO_2 sample from La Flexura (11-B3), give an estimate of the total reproducibility of analyses. For BHVO-1, the reproducibility (here expressed as the 2 standard deviation/mean ratio of the 16 analyses performed during the course of the study) is better than 5% for major element contents, except for N_2O (13%), K_2O (18%), and P_2O_5 (8%), and around 3 and 24% for Sr and Ba, respectively. For 11-B3 sample, this is of the same order, with a maximum of 2.5% for major element contents, except for MnO (5%), K_2O, and P_2O_5 (10%), around 3% for Sr and around 15% for Ba (supporting information Table S1).

Sr and Nd isotope separations and measurements were also carried out at the LMV. Hundred milligrams of sample powders were acid-digested with a HF-HNO_3 mixture and passed through the "cascade" column protocol (Sr Spec, True Spec, and Ln Spec columns) described in *Pin and Bassin* [1992] and *Pin et al*. [1994] after most of the iron had been removed through an AG50X4 column. Total procedure blanks were <1 ng and <0.2 ng for Sr and Nd, respectively. A few samples were also spiked with a ^{150}Nd tracer solution in order to determine their Nd content by isotope dilution. All measurements were made in static mode on a Finnigan Triton thermo-ionization mass spectrometer (TIMS) with relay matrix rotation (also called the virtual amplifier) and double W filaments. A typical run consisted of at least nine blocks of 10 cycles to allow a full rotation of the virtual amplifier system. Isotope ratios were mass-fractionation corrected with $^{86}Sr/^{88}Sr = 0.1194$ and normalized to $^{87}Sr/^{86}Sr = 0.71025$ for the NIST-SRM987 standard; with $^{146}Nd/^{144}Nd = 0.7219$ and normalized to $^{143}Nd/^{144}Nd = 0.511960$ for the Rennes-AMES standard [*Chauvel and Blichert-Toft*, 2001]. Repeated analyses of the two standards during the course of the study gave $^{87}Sr/^{86}Sr = 0.710244 \pm 0.000007$ (2sd, n = 56) and $^{143}Nd/^{144}Nd = 0.511960 \pm 0.000007$ (2sd, n = 44).

3.2. Grain-Size Dependence of Matrix Samples

To assess the influence of particle-size distribution of matrix on measured chemical and isotopic compositions, we passed a large sample (33-M1) through a manual sieve shaker with meshes of 1 and 0.1 mm. The three fractions ($\leq$0.1 mm; 0.1–1 mm; and $>$1 mm, denoted as 33-M1a, 33-M1b, and 33-M1c, respectively) show isotopic compositions in agreement with that of the whole-rock sample when considering error bars of 7×10^{-6} (see above) for Sr-Nd ratios (Figure 3a). Major and trace element content results, however, contrast. Although the large and intermediate size fractions show maximal differences of $\pm$5% compared with the whole-rock matrix sample for major and trace elements analyzed with a similar precision (SiO_2, Al_2O_3, Fe_2O_3, MgO, and Sr), smaller particles ($\leq$0.1 mm) have significantly distinct contents (between 5 and 15% for SiO_2, Al_2O_3, Fe_2O_3, and MgO, and up to 50% for Sr; cf., Figure 3b). Differences are correlated on Harker diagrams (Figures 3c–3f): small, intermediate, and large particle subsamples plot on the general trends defined by the whole set of Socompa deposits. Given the constant Sr-Nd isotopic composition measured in all fractions, variations recorded by major elements thus seem simply to reflect variations in mineral proportions. The fine particle subsample presents a higher proportion of a component with a SiO_2-rich composition (mesostasis?) relative to the intermediate and large grain distributions. Conversely, the latter are consistent with higher amounts of plagioclase and/or augite and/or amphibole. Comparison of all particle sizes thus suggests that major element results, as well as Sr and Ba, depend on sampling. Coupled to reproducibility of major and trace element contents, this implies that very small differences ($\leq$10%) between two

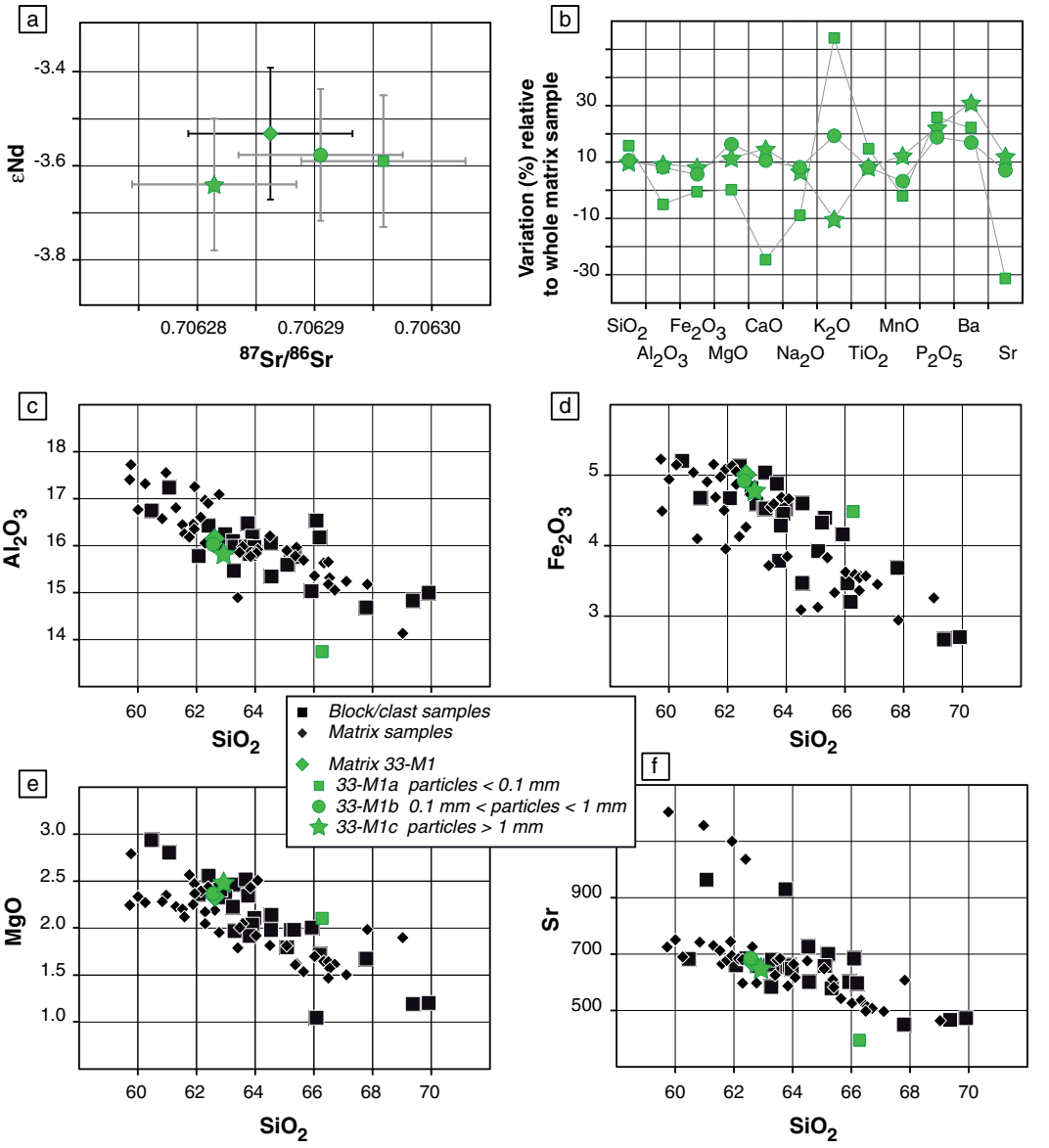

Figure 3. Influence of particle-size distribution of matrix sample 33-M1 on major and trace element, and isotope signatures. (a) εNd versus $^{87}Sr/^{86}Sr$, (b) variations (%) relative to whole-matrix sample for major and trace elements, and (c–f) comparison with all matrix and block samples from the Socompa avalanche deposits in Harker diagrams (wt %). All fractions show reproducible Sr-Nd isotopic compositions but distinct major element contents interpreted as reflecting variable mineral proportions.

samples cannot be considered as significant. Furthermore, beyond the sampling bias, using major element may induce wrong conclusions if granulometric sorting occurs during the avalanche emplacement. Consequently, discussion will be based primarily on Sr-Nd isotopes.

3.3. How Representative Are Matrix Signatures of Individual Outcrops?

We have also checked how representative matrix sampling is of a given outcrop. For this purpose, we have collected several visually identical matrix samples, separated by a few 10s of cm at given locations. An example is illustrated in Figure 4 (outcrop 7). The four matrix samples collected at intervals of 30 cm present Sr-Nd isotope compositions of 0.706291–0.706306 and 0.512451–0.512458, as well as SiO_2 contents ranging from 60.01 to 61.59 wt %. This corresponds to relative variations of 21 ppm, 13 ppm, and 2.6%, respectively. Such values are similar to reproducibilities based on standard measurements (see section 3.1), making differences between them insignificant. Furthermore, the four matrix data points plot within the

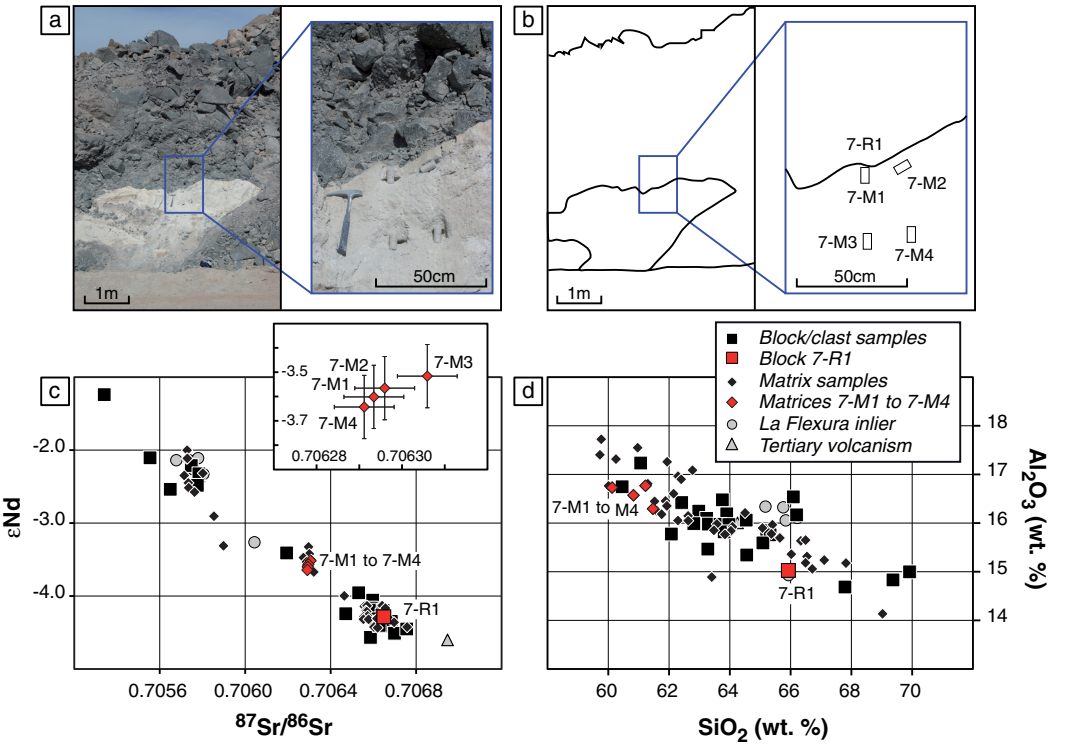

Figure 4. (a) Photograph, (b) schematic field relationship, (c) εNd versus $^{87}Sr/^{86}Sr$, and (d) Al_2O_3 versus SiO_2 diagrams for samples from outcrop 7 (distal zone of the avalanche, see Figure 2 for exact location). The four matrix samples, 7-M1 to 7-M4, show only minor isotope and major element variations that can be considered as insignificant with respect to analytical uncertainties and reproducibilities. Block sample at contact (7-R1), however, presents significantly distinct isotopic and chemical signatures. Note the ingestion of the lava into the matrix (left of the caption).

trend defined by the entire set of Socompa deposits in the Al_2O_3 versus SiO_2 diagram, suggesting that part of the major element variability could be related to varying proportions of small, intermediate, and/or large grain size particles in the four matrix samples. However, massive blocks of dacite at the contact show differences far higher than analytical uncertainties for both isotopes and major elements. Thus, the outcrop 7 test, duplicated at locations 8 and 9 with the same results (supporting information Table S1), shows that matrix samples are representative of one to several meter-sized matrix outcrops with respect to analytical uncertainties for both isotopes and major elements.

4. Geochemical Compositions of Socompa Debris-Avalanche Deposits and Basement

Sample deposits show similar major element variations, whatever their type. Massive blocks and clasts have SiO_2 contents ranging from 61.40 to 70.10 wt %, recalculated on an anhydrous basis. All but two samples fall within the andesite to trachy-andesite and dacite to trachydacite fields when plotted in the total alkali-silica diagram (Figure 5). The two exceptions are rhyolitic clasts coming from the same location (outcrop 10). Matrix samples have similar SiO_2 (61.19–69.79 wt %). Their alkali contents (Na_2O+K_2O), however, are lower overall than those of rock samples; they all plot in the andesite and dacite fields, except four samples which are categorized as trachydacites. La Flexura samples have narrower, dacitic compositional ranges for seven of the eight samples; only 11-B3 is an andesite. Rock and matrix samples divide into medium-K and high-K types, the former being predominant, whereas La Flexura samples are all medium-K (supporting information Figure S2). Rock samples and clasts show low loss on ignition (LOI) values ranging from 0.05 to 2.10 wt % (mean = 0.76 wt %). Conversely, matrix and La Flexura samples have higher LOI values of 0.20–5.55 wt % (mean = 1.91 wt %) and 1.23–7.85 wt % (mean = 3.35 wt %), respectively. These differences may either reflect the higher alterability, even in an arid climate, of crushed material compared to rock blocks or

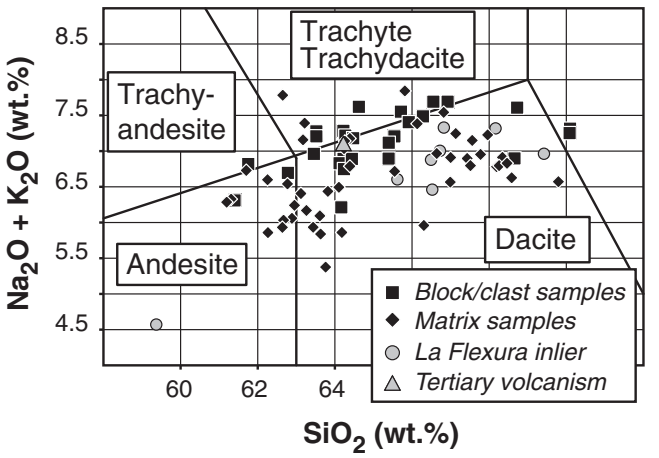

Figure 5. Total alkali-silica diagram [*Le Maître*, 2002] for Socompa debris-avalanche deposits, La Flexura inlier, and tertiary volcanism.

suggest water input into matrix samples. The Chemical Index of Alteration (CIA) quantifies the extent of weathering (based on conversion of feldspar minerals) of a given rock [*Nesbitt and Young*, 1982]: fresh samples show CIA $\leq$ 50, whereas altered ones have higher values of up to 100. Socompa rock and matrix samples have quite similar ranges of CIA, from 45.8 to 49.3 and from 45.4 to 53.4, respectively (supporting information Figure S3a). The upper limit for the matrix samples is set by a single sample; excluding it results in a range of 45.4–50.4. This suggests that all samples are unaltered, or only weakly altered. This is confirmed by the calculation of the Weathering index (W) [*Otha and Arai*, 2007]. Our samples do not deviate from the unweathered igneous rock trend in the MFW ternary diagram (where M, F, and W represent the mafic source, felsic source, and weathered material; see supporting information Figure S3b).

The Tertiary sample (14-R1), collected from the Negrillar lavas to the north of the studied deposits (Figure 2), has no relationship with the debris avalanche (there is no evidence for a genetic link with Socompa volcano either). It has a dacitic composition similar to that of average rock samples. Unconsolidated sediment samples show contrasted results: 25-S1 is Mg-rich, whereas 4-S1 and 12-S1 are Ca-rich.

Measured $^{87}Sr/^{86}Sr$ and $^{143}Nd/^{144}Nd$ isotope ratios for Socompa avalanche deposits range from 0.705340 to 0.706758 and from 0.512404 ($\varepsilon Nd = -4.57$) to 0.512574 ($\varepsilon Nd = -1.24$) (εNd is the deviation from the Chondritic Uniform Reservoir (CHUR) evolution line in parts per 10,000), respectively. No radioactive decay correction is applied to values as deposits all come from Socompa volcano, whose activity is Quaternary [*Mamani et al*., 2010]. Sample values of $^{143}Nd/^{144}Nd$ (εNd) decrease with increasing $^{87}Sr/^{86}Sr$. Matrix and rock deposit values overlap, while the three Toreva samples (16-R1, 35-R1, and 36-R1) have among the most radiogenic Sr ratio values (Figure 6). La Flexura samples also plot along the Sr-Nd anticorrelation, but their variation ranges are less than those of Socompa deposits, being confined to rather low $^{87}Sr/^{86}Sr$ (0.705677–0.706043) and high $^{143}Nd/^{144}Nd$ ratios (0.512471–0.512530). The Tertiary sample from the Negrillar lavas and the unconsolidated sediment samples (12-S1 and 25-S1) show the highest $^{87}Sr/^{86}Sr$ ratios. The Tertiary lava occupies an end-member position with respect to Socompa deposits, while the magnesium-rich and calcium-rich unconsolidated sediments lie off the trend.

5. Discussion

5.1. Outcrop-Scale Relationships Between Matrix and Block Samples and Implications for Dynamics

Strontium-87/^{86}Sr and $^{143}Nd/^{144}Nd$ isotope ratios define a negative trend for block/clast samples (Figure 6). Similarly, SiO_2 correlates negatively with all other major elements (Figures 3c–3f) except K_2O (positive correlation). Matrix samples define very similar correlations to the blocks in both $^{143}Nd/^{144}Nd$ versus $^{87}Sr/^{86}Sr$ and Harker diagrams. Hence, variations in the chemical and isotopic compositions of matrix samples seem to result from a simple, mechanical mixing of Socompa rocks after crushing. However, major elements and isotope ratios do not vary together. Such a decoupling suggests that matrix samples result from numerous mixing events with variable end-members. In the following sections, we discuss relationships between matrix and block samples in the key sectors of the avalanche in order to better understand its dynamics.

5.1.1. The Proximal Zone

Field observations and satellite images suggest that the proximal zone corresponds to strong stretching of the avalanche. Deposits form well-defined, parallel colored bands in the central part of the sector (Figure 2)

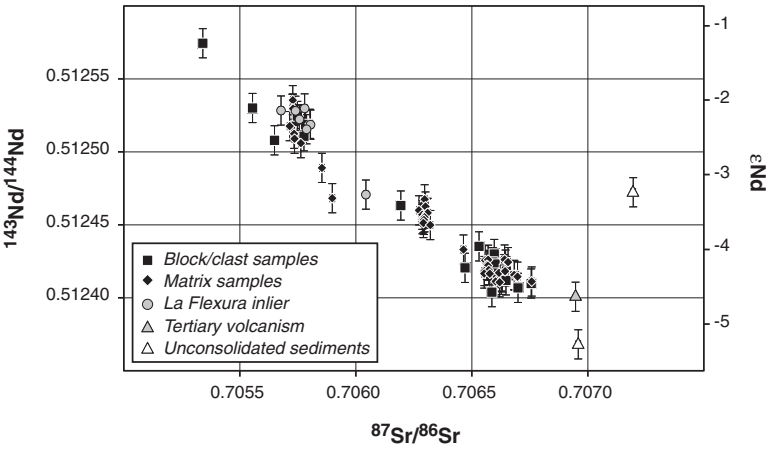

Figure 6. Comparison of matrices with blocks/clasts from the Socompa avalanche deposits on a $^{143}Nd/^{144}Nd$ (εNd) versus $^{87}Sr/^{86}Sr$ diagram. εNd is the deviation from the Chondritic Uniform Reservoir (CHUR; with $^{143}Nd/^{144}Nd_{Today} = 0.512638$) [cf., *Jacobsen and Wasserburg*, 1984] evolution line in parts per 10,000. La Flexura-like basement samples, as well as sample 14-R1, representative of regional tertiary volcanism, and local unconsolidated sediments are also shown. All samples except unconsolidated sediments plot on the same, well-defined, negative correlation.

indicating a unique direction toward the north-west. Rocks at the surface of each band seem to be homogeneous (in terms of nature and mineralogy) [*Francis et al*., 1985; *Wadge et al*., 1995; *van Wyk de Vries et al*., 2001; *Kelfoun et al*., 2008].

Our analyses show that matrix samples collected from this area have homogeneous compositions within a given colored band, similar to the blocks. For example, matrix samples 17-M1, 18-M1, 19-M1, and 33-M1 that were collected in a light blue, elongated area (Figure 2) show similar isotope ratios (supporting information Table S1). This is also true for 9-M1–9-M4 and 37-M1, which belong to the greenish band located immediately to the east. Their isotope signatures are similar, although different from those of the former samples. Hence, samples from distinct color areas present different isotopic compositions, even if they are located near one another.

Our analyses also show that matrices and blocks sampled in contact with each other have identical isotope ratios, although matrices present a globally white color, contrary to neighboring blocks that give the color of the bands on the satellite image. This is observed at outcrops 9 (supporting information Table S1) and 20 (gray band located to the east of the greenish one (Figure 2)). This result indicates that matrices are derived from surface blocks by simple crushing. All avalanche outcrops show that the matrix dominates below the zero to few meter-thick surface crust of deposits, which suggests that crushing operated over most of the deposit thickness (probably more than 90% of the thickness).

Differences in Sr-Nd isotope compositions observed in matrices from the parallel bands (light blue, greenish, and gray; Figure 2) show that lateral mixing is limited in the proximal zone. The similarity of ratios between blocks and matrices in a given colored band also suggests that there is no mixing with rocks crushed at greater depth, regardless of their origin (rocks from the Socompa volcano or from the basement) unless they have the same composition.

Outcrop 20 is of particular interest as it also illustrates how difficult it is to distinguish between compositions on the field. Here the three visually distinct matrices in contact have the same isotope composition (Figure 7). The visual distinction between them could be related to different degrees of alteration. The uppermost matrix (sample 20-M3) is red-brown, compared to gray and light gray matrices sampled directly below (20-M1 and 20-M2), which could represent alteration of iron minerals. Their distinct appearances could be also related to the proportion of blocks disseminated through the matrices, or they simply reflect original matrix materials that were initially in contact (before the avalanche) but were not mixed by crushing.

The southwest edge of the proximal zone is a more complex sector, whose structures are not easy to interpret [*Kelfoun et al*., 2008]. The initial direction of stretching is perpendicular to the local slope; thus, movement was probably not unidirectional. An example of the relationship between blocks and matrices in contact is given

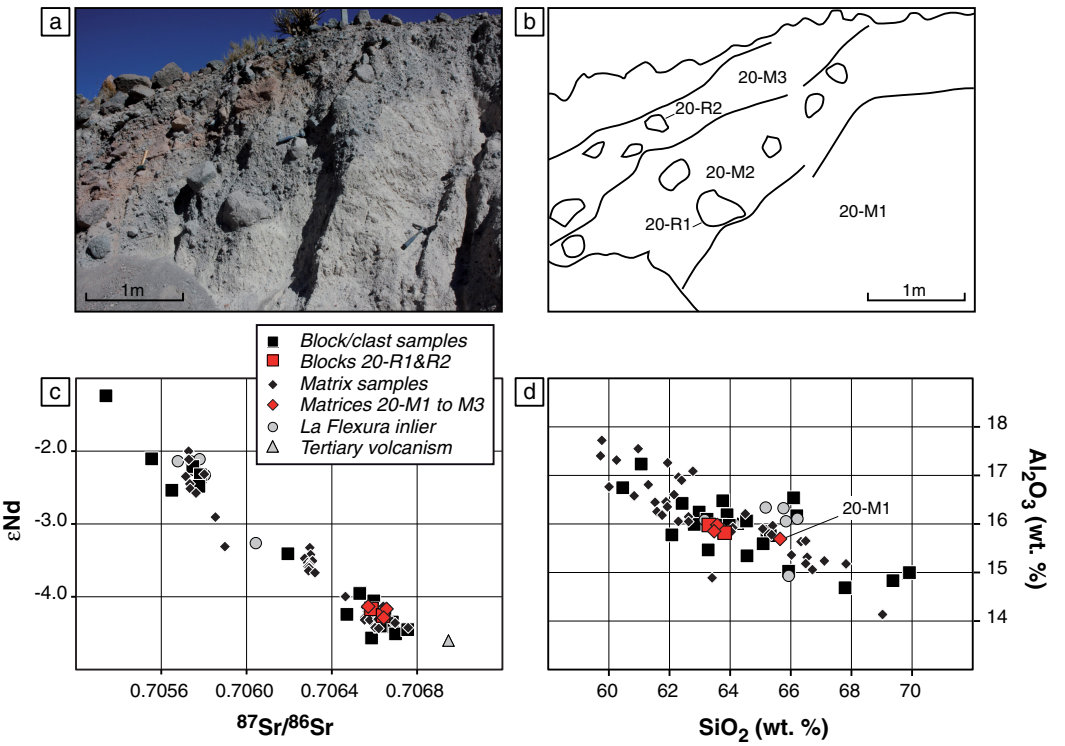

Figure 7. (a) Photograph, (b) schematic field relationship, (c) εNd versus $^{87}Sr/^{86}Sr$, and (d) Al_2O_3 versus SiO_2 diagrams for samples from outcrop 20 (proximal zone of the avalanche, see Figure 2 for location). The three matrix layers, 20-M1 to 20-M3, show distinct field characteristics (presence/absence of clasts, color), but very similar isotopic compositions, as do the two block samples (20-R1 and 20-R2).

by outcrop 27 (Figure 8). Here a visually homogenous rock cover caps two distinct matrices. In the field, the pink matrix (27-M1) seems to result from the incorporation of red blocks (represented by sample 27-R1) into a white matrix (27-M2). However, Sr and Nd isotope compositions measured for 27-M1 are not intermediate between those of samples 27-M2 and 27-R1. In fact the white matrix (27-M2) and the rock cover (27-R1) have very similar isotope signatures, whereas the pink matrix (27-M1) has significantly distinct Sr-Nd ratios. Thus, if 27-M1 is related to 27-M2 and 27-R1 through a mixing process, an unidentified, unsampled component is needed to explain its chemical composition. Alternatively, we can interpret the 27-M1 matrix as a very localized event, resulting from the crushing of rocks with a distinct isotope signature to that of the 27-R1 sample. This possibility highlights the difficulty of limited sampling of representative rock fragments/blocks. This also illustrates that field observations should be made with caution in relation to chemical compositions.

5.1.2. The Distal Zone

In the distal region, the avalanche deposits were laid down and then subjected to a back surge, which created large shear zones and stretching. These large structures allow the matrices to be observed in areas where blocks cap the whole surface. For example, outcrop 7 shows the contact between a white matrix and a dismantled lava block unit (Figure 4). There, the disaggregation of the lava unit and its ingestion into the matrix are visible. However, the four matrix samples collected at intervals of 30 cm (7-M1–7-M4) show exactly the same isotopic composition regardless of their distance from, and direction in relation to, the block chosen as representative of the lava unit (7-R1), and the block and matrices have contrasting major and trace element and isotope signatures. Such differences preclude the matrices being derived from the adjacent blocks by a simple crushing process, but suggest a binary mixing between block 7-R1 and an unidentified, unsampled component. The geochemical homogeneity of the matrix indicates large-scale mixing to incorporate the lava so efficiently into the matrix.

The same kind of relationship is observed at outcrop 8 (Figure 9), where a thin, ~50 cm, layer of fragmented rocks, here represented by sample 8-R1, caps a thick layer of matrix (more than a few meters thick). Again, Sr-Nd isotope compositions of matrix samples 8-M1 and 8-M2 are similar, but distinct from those of block 8-R1, collected at, or close to, the contact. Such features probably indicate the complete mixing of the lower

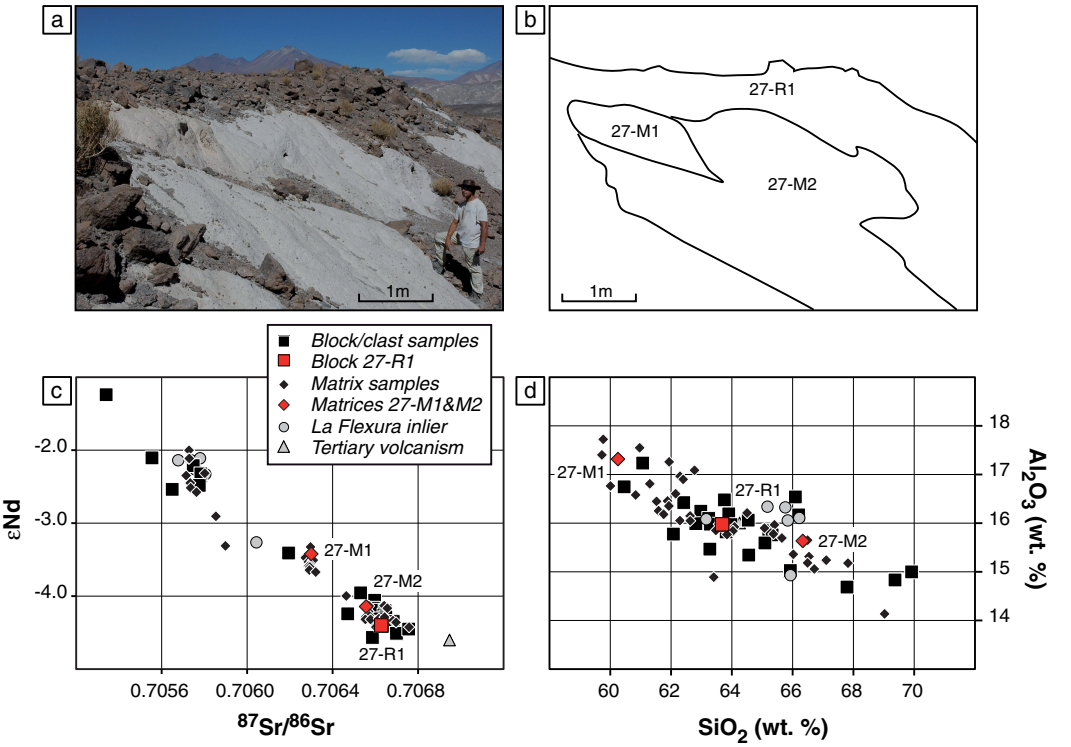

Figure 8. (a) Photograph, (b) schematic field relationship, (c) εNd versus $^{87}Sr/^{86}Sr$, and (d) Al_2O_3 versus SiO_2 diagrams for samples from outcrop 27 (see Figure 2 for location). The southwest edge of the proximal zone of the avalanche shows complex relationships between matrices and blocks in contact compared to the central part where both types of samples have identical isotope ratios.

part of the rock cap into the underlying matrix. Hence, more than 90% of the deposit thickness seems to have been affected by mixing in the distal area. It should also be noted that the matrix samples collected at outcrops 7 and 8 have distinct Sr-Nd ratios, arguing for a heterogeneous distal zone and thus a heterogeneous matrix at the scale of a few km.

5.1.3. The Frontal Zone

The frontal lobe of the avalanche is a specific zone whose surface contains a high proportion of matrix material, as is also the case for frontal levees from the north-northwest region. Structures are not clearly defined, and outcropping rocks seem to be heterogeneous. We focused on outcrop 13, located at the front of the avalanche deposits and representative of this area. There, a great variety of rock fragments disseminated into the matrix can be observed (Figure 10). Samples 13-R1–13-R11 show Sr-Nd isotope ratios spanning the whole range of measured compositions for Socompa avalanche deposits, whereas matrix sample 13-M1 has an isotopic signature close to that of La Flexura samples. Major element contents determined for these samples show similar ranges, so the matrix could result from the incomplete mixing of rocks with isotopic compositions similar to 13-R1/R11. Alternatively, 13-M1 could result either from the mixing of at least two unsampled components or from the crushing of La Flexura-like material. In either case, the distribution of blocks in the matrix indicates that the frontal lobe was affected by strong mingling reaching down to the underlying deposits.

5.1.4. The Median Escarpment

The median escarpment delimits the backward movement of the avalanche toward the south-east. There, the matrix samples we collected at the contact are not easy to ascribe an origin to. For example, outcrop 10 is composed of two color-contrasted matrices (a pink matrix: samples 10-M1 and 10-M2, and a blue matrix: samples 10-M3 and 10-M4) containing three main types of small clasts (a few cm in size): pink clasts (sample 10-R1) are dispersed in pink matrix 10-M1, and dark (10-R2) and light (10-R3) fragments in blue matrices 10-M3 and 10-M4 (Figure 11). Our analyses show that the matrices of distinct colors are homogeneous: Sr-Nd ratios, and major and trace element contents, show similar values for samples 10-M1 and 10-M2, and for

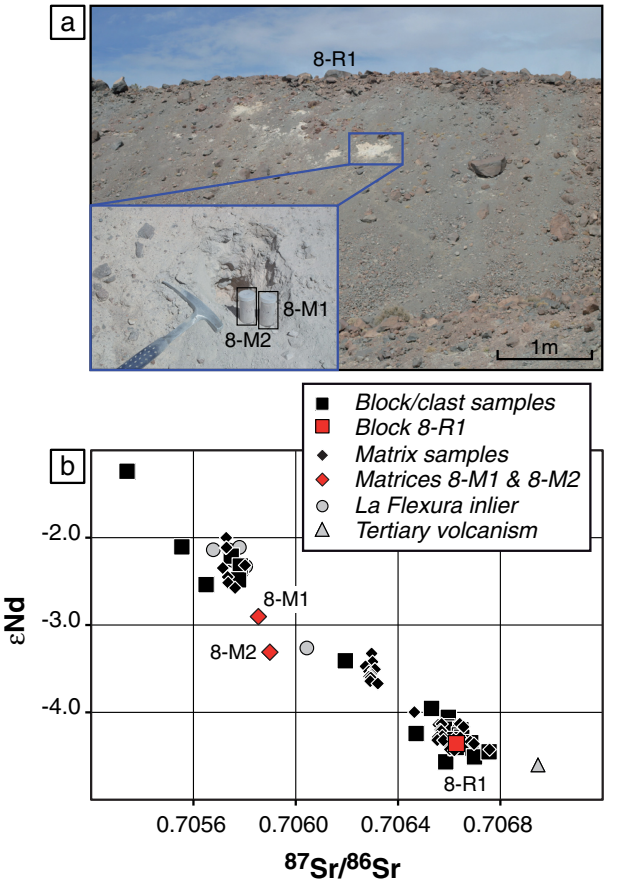

Figure 9. (a) Photograph and (b) εNd versus $^{87}Sr/^{86}Sr$ diagram for samples from outcrop 8 (distal zone of the avalanche, see Figure 2 for exact location). Note there is only a thin, ~50 cm, layer of fragmented rocks, here represented by sample 8-R1, over a thick—more than a few meters—layer of matrix (samples 8-M1 and 8-M2). As for outcrop 7, matrices and block in contact present significantly distinct isotopic signatures.

samples 10-M3 and 10-M4. The two types of matrices, however, present significantly distinct isotopic and chemical compositions from each other. Thus, there is no interaction between the two matrices, which is in agreement with their very sharp contact. The three color-based types of clasts also have distinct signatures, not only from each other but also when compared with matrix samples. Thus, neither of the two matrices can be explained by the simple crushing of material resembling one of the three types of clasts (pink, dark, or light color). For example, the pink matrix cannot result from crushing of pink clasts. Again, this illustrates that field observations should be made with caution.

In the εNd versus $^{87}Sr/^{86}Sr$ plot (Figure 11c), the five samples collected at outcrop 10 define a negative correlation. The relative location of matrix and block/fragment samples on this diagram suggests that matrices 10-M1 and 10-M2 result from the binary mixing between rocks with either 10-R1 and 10-R2 or 10-R1 and 10-R3 compositions, whereas matrices 10-M3 and 10-M4 could result from mixing between either 10-R1 and 10-R2 or 10-R2 and 10-R3. In this scenario, whatever the two end-members involved, the mixing must have been mechanical and incomplete as fragments still exist to be sampled. However, equivalent relationships to those observed for isotopes are not found on an Al_2O_3 versus SiO_2 diagram; for example, the three rock fragments show higher SiO_2 contents than matrix samples (Figure 11d). Thus, if mixing were to be the process which resulted in the two matrices (pink and blue) at outcrop 10, at least one of the components of the mixing remains unidentified and consequently unsampled at this location. Alternatively, the two matrices might have no relationship to each other, or to the blocks or clasts. Whatever the explanation, this shows that the homogeneous matrix contains, or was formed by, rocks of various origins. Thus, the avalanche was fluid or shaken enough to allow mechanical mixing, as also inferred for the outcrops in the distal zone. Our study also indicates that strong mixing affected the deposits up to their surface. Homogeneous matrices were formed by the grinding of various rocks, as testified by remaining clasts that are also homogeneously distributed throughout the matrices. The sharp contact between the two matrices (pink and blue) indicates that the strong mixing phase was followed by a phase during which mixing was no longer possible. The matrices were then put in contact by granular faults in a material that henceforth behaved in a brittle manner.

5.2. Basement Involvement in Debris-Avalanche Deposits

5.2.1. La Flexura-Like Basement Involvement

Some of the outcrops described in previous sections suggest the involvement of an unidentified component in matrix samples. Here we look into the possibility that the debris avalanche eroded basement rocks

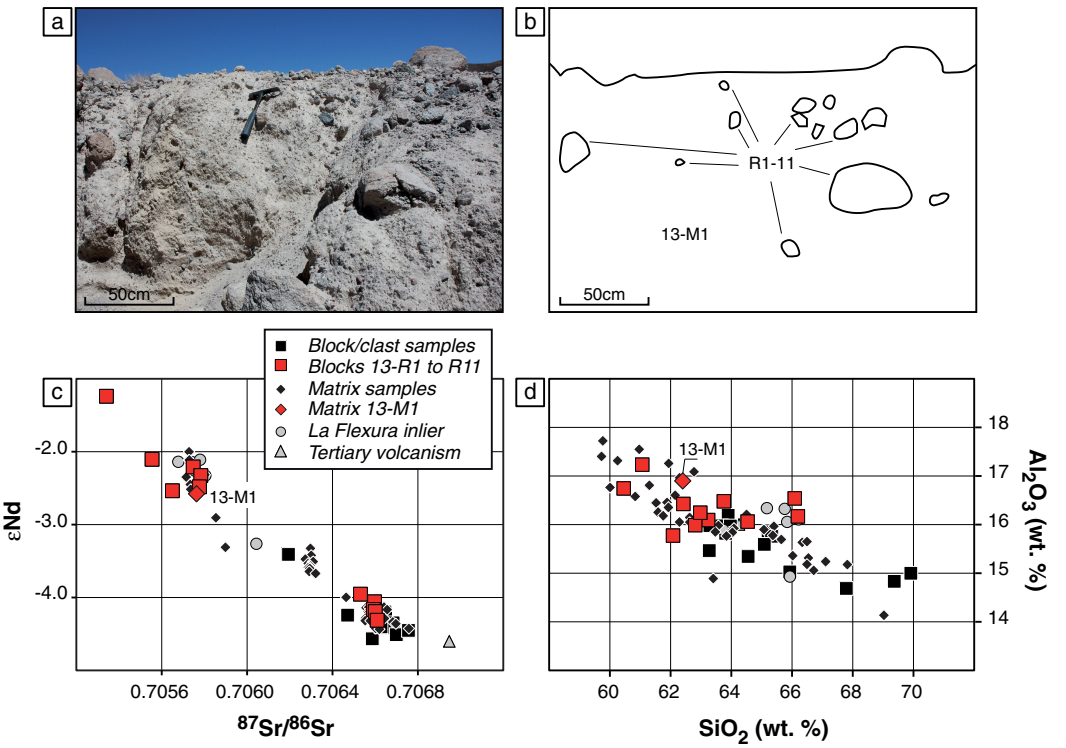

Figure 10. (a) Photograph, (b) schematic field relationship, (c) εNd versus $^{87}Sr/^{86}Sr$, and (d) Al_2O_3 versus SiO_2 diagrams for samples from outcrop 13 (front part of the avalanche, see Figure 2 for exact location). Eleven visually distinct rock samples, namely 13-R1 to 13-R11, have been collected into matrix 13-M1; their compositions span the whole range of variations of Socompa avalanche deposits. Matrix 13-M1 has an isotopic signature close to that of La Flexura samples.

of the Socompa volcano and incorporated 60–80% within it [*Wadge et al.*, 1995; *van Wyk de Vries et al.*, 2001]. For this purpose, we assume that each matrix sample results from mixing between crushed Socompa rocks from the same outcrop and La Flexura-like material, and we determine mixing proportions to fit our data. We consider both major element and isotope calculations, which must both give similar mixing proportions. Results show that mixing with La Flexura-like material in proportions ranging from 15 to ~95% can explain the chemical and isotopic compositions of several matrix samples, provided that all La Flexura-like compositions are considered (from andesite to dacite; see Figure 12). Others, however, cannot be modeled by such mixing. For example, matrix sample 27-M2 does not fall on a trend joining La-Flexura and block 27-R1 from outcrop 27 (located in the proximal zone; see section 5.1.1). Moreover, a few outcrops have adjacent matrix and rock samples with similar geochemical characteristics, thus making mixing with La Flexura-like basement material unnecessary (outcrops 9 and 20 also located in the proximal zone). Thus, our data do not exclude La Flexura-like basement assimilation by the Socompa avalanche, but it appears to be not nearly as significant as previous studies suggest. This conclusion is based on the hypothesis that La Flexura samples are representative of the whole Socompa basement, but it should be noted that the La Flexura inlier was also used as a reference by previous studies to estimate the degree of involvement of Socompa basement in deposits.

5.2.2. Monturaqui Unconsolidated Sediment Incorporation

Ca-rich and Mg-rich unconsolidated sediments have been also sampled to the north and east of the Socompa avalanche deposits. Measured isotopic compositions show high Sr ratios and low Nd ratios ($^{87}Sr/^{86}Sr = 0.706959–0.707195$ and $^{143}Nd/^{144}Nd = 0.512368–0.512474$), so average sediments can be plotted as an end-member for Socompa matrix and block samples in the $^{143}Nd/^{144}Nd$ versus $^{87}Sr/^{86}Sr$ diagram (Figure 6). Thus, it could be proposed that matrix samples result from binary mixing between Sr unradiogenic material from Socompa volcano and unconsolidated sediments (instead of basement rocks). In this case, the mass proportions required to explain intermediate matrix compositions (i.e., $^{87}Sr/^{86}Sr \sim 0.706300$) are around 30% when considering $^{87}Sr/^{86}Sr$ isotopic ratios of 0.706959 (Ca-rich sample) and

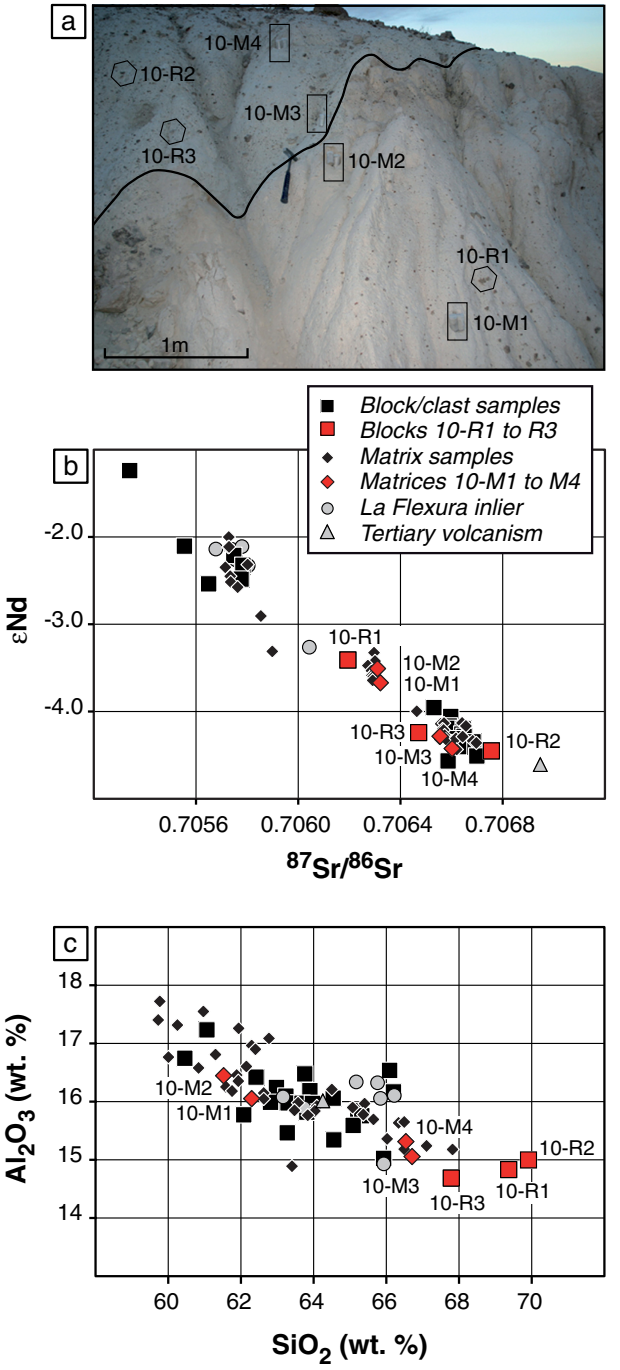

Figure 11. (a) Photograph, (b) εNd versus $^{87}Sr/^{86}Sr$, and (c) Al_2O_3 versus SiO_2 diagrams for samples from outcrop 10 (median escarpment, see Figure 2 for exact location). Matrix samples divide into pink (10-M1 and 10-M2) and blue (10-M3 and 10-M4) matrices. Pink clast 10-R1 is collected in matrix 10-M1, whereas 10-R2 and 10-R3 are samples of disseminated, dark, and light rock fragments from 10-M3 and 10-M4 blue matrices. Matrices of distinct colors are homogeneous. Both types, however, present significantly distinct isotopic and chemical compositions. In the same way, the three types of clasts show distinct signatures, not only between the groups but also when compared with matrix samples.

0.705340 (which corresponds to the least Sr radiogenic sample 13-R3), together with Sr contents of 2345 and 685 ppm for the sediments and the Socompa Sr unradiogenic end-member, respectively. Such mass proportions result in maximum SiO_2 contents of ~58 wt % for a rhyolite-like starting composition (calculations are carried out with SiO_2 = 29.5 wt % for Ca-rich unconsolidated sediments; supporting information Table S1) and thus do not explain the andesitic and dacitic compositions of most matrix samples. The same conclusions are reached using Mg-rich samples, where mixing proportions of ~68% can reproduce the isotopic ratios of matrices with an intermediate composition, but this gives maximum SiO_2 contents of 25.5 wt %, far below that of the observed dacitic and andesitic compositions. Thus, if the avalanche eroded unconsolidated sediments from the Monturaqui basin, there is no evidence of them at the deposit surface. Alternatively, this could suggest that erosion was very low, despite the fact that the avalanche was emplaced onto a low-strength substratum.

5.3. Internal Dynamics of the Avalanche

We quantify the level of heterogeneity of a given outcrop using the Sr-Nd isotopic difference ($D_{Sr\text{-}Nd}$) between matrices and blocks/clasts that were sampled at a given location. This involves calculating the geochemical distance between two samples (one matrix and one block) on the $^{143}Nd/^{144}Nd$ versus $^{87}Sr/^{86}Sr$ plot using a least squares-type formula

$$D^2_{Sr-Nd} = \left[\left(^{87}Sr/^{86}Sr\right)_{C/B} - \left(^{87}Sr/^{86}Sr\right)_M\right]^2 / \sigma^2_{Sr} + \left[\left(^{143}Nd/^{144}Nd\right)_{C/B} - \left(^{143}Nd/^{144}Nd\right)_M\right]^2 / \sigma^2_{Nd} \quad (1)$$

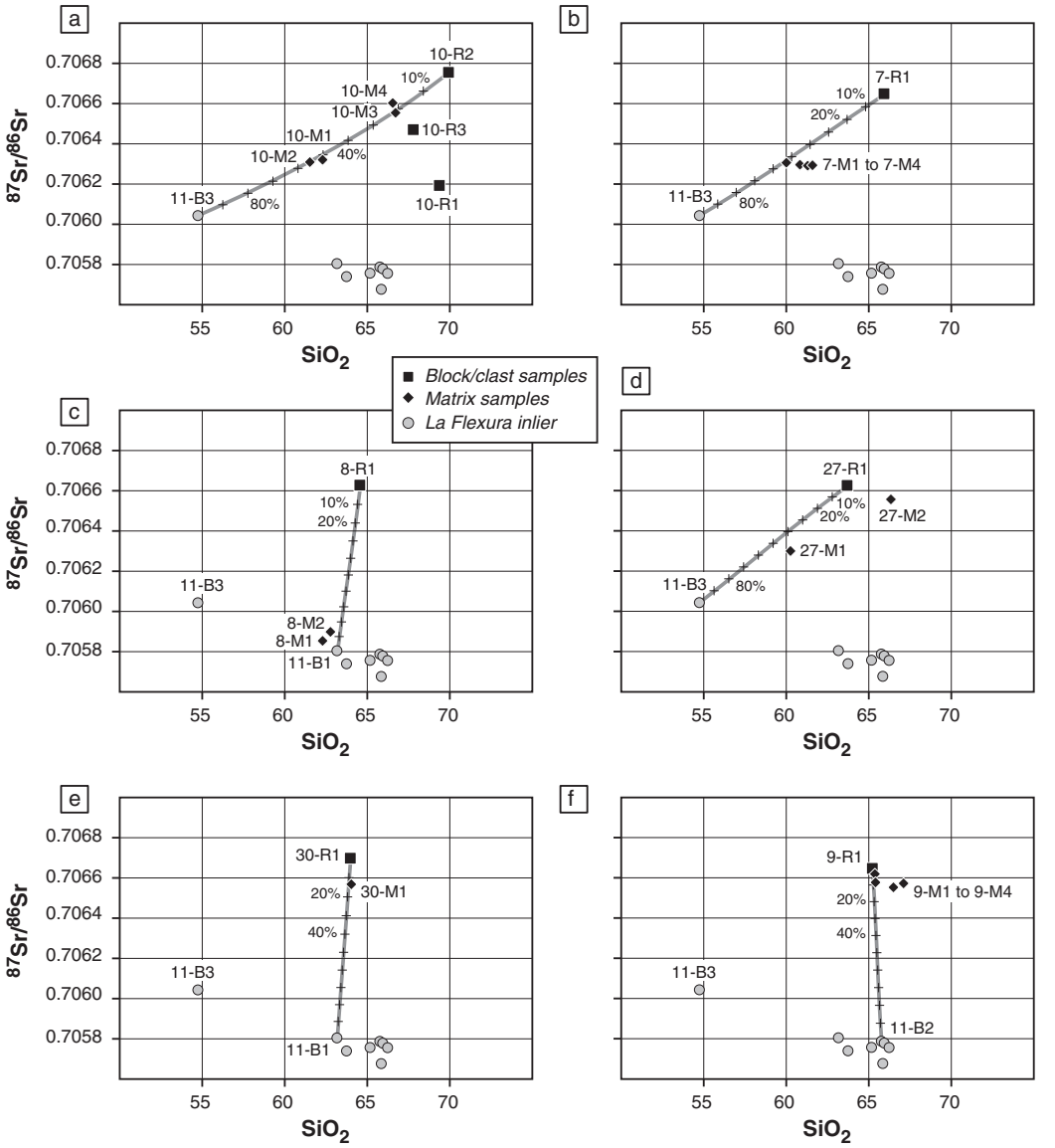

Figure 12. Strontium-87/^{86}Sr versus SiO_2 contents for La Flexura samples together with blocks and matrices from (a) outcrop 10, (b) outcrop 7, (c) outcrop 8, (d) outcrop 27, (e) outcrop 30, and (f) outcrop 9. Chemical and isotopic compositions of some matrix samples in contact with blocks displaying distinct contents and isotopic ratios can be explained by a binary mixing of materials resulting from the crushing of blocks and La Flexura-like samples. In this case, mixing proportions range from 15 to 95% of La Flexura-like material. Such a mixing, however, does not explain all matrix samples (for example, 27-M2, 9-M3, and 9-M4). For outcrops 7, 10, and 27, the only suitable sample for the basement end member is andesitic sample 11-B3 that has clearly different major element and isotope compositions relative to other La Flexura samples.

C/B refers to clast/block samples and *M* to matrices, and σ_{Sr} and σ_{Nd} are the standard deviations of our $^{87}Sr/^{86}Sr$ and $^{143}Nd/^{144}Nd$ measurements determined for blocks and matrices. Analogue distances are usually determined to assess the quality of a model by comparing modeled values and measured ones [e.g., *Debaille et al*., 2006]. Where there is more than one possibility for the calculation (i.e., there is more than one combination of matrix and block samples for a given outcrop), distances for all combinations are determined.

Results show marked variations, from 0.04 to 3.04 (normalized Sr-Nd isotopic scale), illustrating the various relationships observed between blocks/clasts and matrices: both types of sample can indeed show identical (or very similar) isotopic compositions as well as distinct ones (see section 5.1). Figure 13a illustrates the level of heterogeneity for each outcrop, or $D_{Sr\text{-}Nd}$ value, as a function of the linear distance from Socompa's

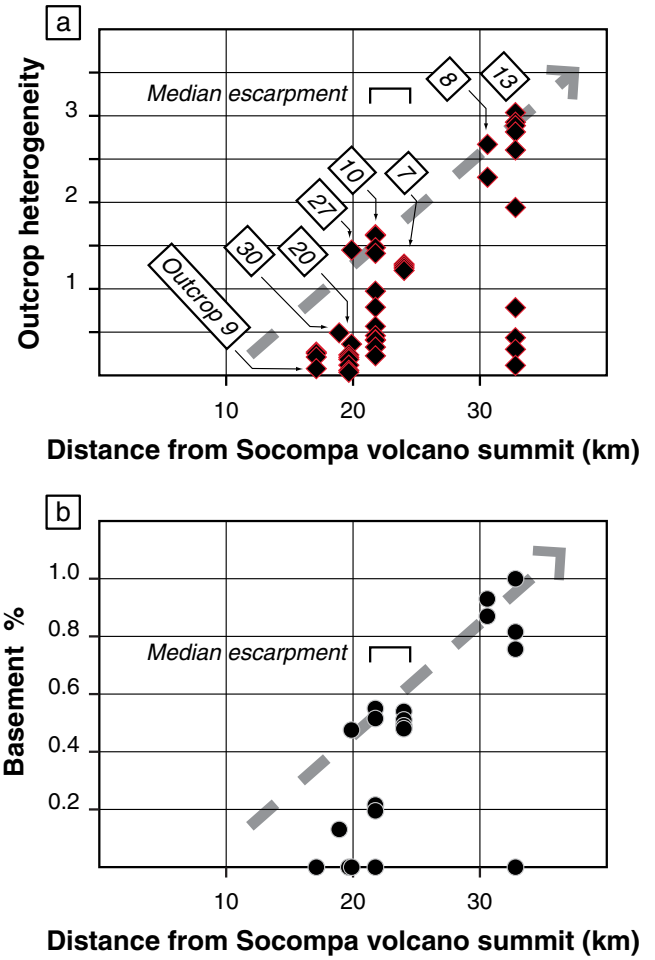

Figure 13. (a) Outcrop heterogeneity (here defined as the Sr-Nd isotopic distance between matrices and associated blocks/clasts in the $^{143}Nd/^{144}Nd$ versus $^{87}Sr/^{86}Sr$ plot) and (b) La Flexura-like basement proportions in matrix samples, as a function of the distance from Socompa's summit (UTM coordinates: WGS84; zone 19S; easting = 576500; and northing = 7301634). Numbers in italics refer to outcrops.

summit. No correlation between the two variables is observed when all the data are considered. However, maximum values of $D_{Sr\text{-}Nd}$ increase with distance from Socompa's summit. Assuming that the latter distance is a good proxy for the distance of movement, this allows several constraints relative to the internal dynamics of the Socompa debris avalanche during motion to be identified (schematized in Figure 14).

1. In the proximal zone of the avalanche, vertical and horizontal mixing is either limited to the deeper part of deposits, or is nonexistent. Sampled matrices and surface blocks show similar chemical and isotopic compositions, which results in a low $D_{Sr\text{-}Nd}$ value (as observed, e.g., at outcrop 9). This feature seems to be valid for most of the deposits located south of the median escarpment (Figure 2) as demonstrated by the chemical and isotopic homogeneity of matrices along colored bands of the Landsat image (e.g., samples 17-M1, 18-M1, 19-M1, and 33-M1, which were collected in the light blue band; see section 5.1.1).

2. North of the median escarpment, matrices record mixing of at least two components. Such mixing is more efficient than that affecting deposits in the proximal zone: we now observe a decoupling between matrices and blocks/clasts in terms of chemistry (see e.g., outcrops 7 and 8; Figures 4 and 9).

3. At the debris-avalanche front, the level of deposit heterogeneity continues to increase and outcrops show matrices involving the greatest variety of blocks/clasts in terms of chemical and isotopic composition (outcrop 13; Figure 10). These matrices could result from the mixing of one (or any) of the sampled rocks. In this case, mixing is incomplete as rocks are incorporated whole into the matrix rather than being totally assimilated. Alternatively, matrices could correspond to La Flexura-like basement material. Thus, there would be mingling relationships between rocks and matrices rather than mixing. A hybrid version might also exist between these two alternatives.

Figure 13b shows the proportions of assimilated, La Flexura-like basement material that can be calculated for matrix samples (see section 5.2.1) as a function of the distance from Socompa's summit. As was found for the level of outcrop heterogeneity, there is no real relationship between these two parameters. However, maximum proportions again increase with distance from the summit. This suggests either a higher proportion of La Flexura-like material at the front of the deposit, or a more efficient mixing related to a higher distance of motion permitting La-Flexura-like material to reach the deposit surface.

Finally, superimposed onto these large-scale dynamics are the effects of granular faults mobilised during avalanche emplacement. These put matrices with distinct histories into contact on a local scale. It must also

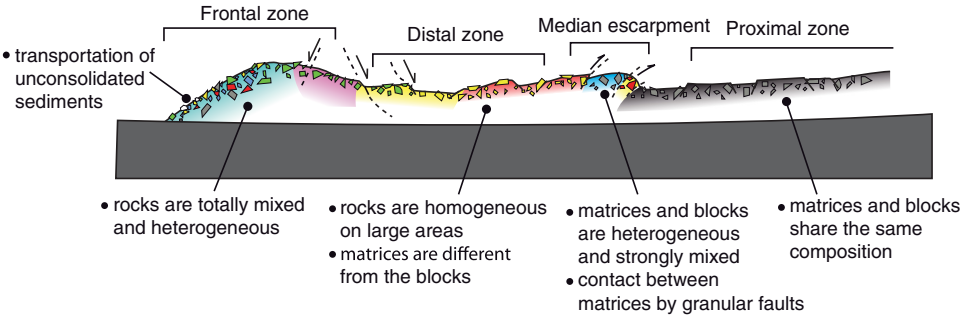

Figure 14. Schematic cartoon showing the key sectors of the avalanche together with conclusions drawn from our geochemical study.

be noted that evidence for mingling (Figures 10 and 11) at the surface shows that the material constituting the avalanche must have been fairly fluid in the top level of the deposits, at least during part of the emplacement period. It also suggests that, for the uppermost part of the avalanche, there was not enough collisional energy and/or stress anisotropy to crush and totally assimilate fragments of blocks (or clasts).

6. Conclusions

Chemical and isotopic analyses of the main constituents of the Socompa debris-avalanche deposits reveal a great variety of compositions, regardless of the type of material studied, i.e., matrices or blocks. Such compositions define unique and clear correlations on isotope and major element variation diagrams, but they do not show a straightforward relationship with the geographical location of samples. This results from their double origin: compositions reflect mixing of crushed material after (and/or during) the collapse of Socompa, as well as differences inherited from Socompa magmas.

Our main conclusions concern the relationships between blocks and matrices in contact. There is no simple relationship between compositions of both types of sample. They can show very similar compositions as well as very distinct ones, which is sometimes inconsistent with field observations. For example, matrices and blocks with distinct, macroscopic aspects (colors and granulometries) can be very similar in terms of both Sr-Nd ratios and major and trace element contents. On a bigger scale, our results confirm the working hypothesis of *Wadge et al.* [1995] and *Kelfoun et al.* [2008] that Landsat images are a powerful tool for identifying rocks of a similar nature (where the climate favors deposit preservation). This last observation must be balanced for matrices. The latter formations indeed present a globally white color and hence are difficult to distinguish from each other. Conversely, isotope geochemistry appears to be a powerful tool for matrix determination.

Matrix samples do not show compositions consistent with that of the La Flexura-like Socompa basement, except for matrices located at the deposit front. If mixing involved basement rocks, then their contribution is variable and it possibly increases from source to front in the surface deposits of the avalanche.

At large scale, the level of heterogeneity of deposits is increasing with the distance from the Socompa edifice summit. This is a completely new result that was never shown by previous numerical and laboratory models. This was not put into evidence by field observations either.

Matrix samples show constant compositions over long distances, from the source to the median escarpment (∼15–20 km). This suggests that there was either no mixing over this distance or no evolution of mixing conditions during motion. At the front, however, we observe a much greater diversity of block/clast samples (with distinct compositions) in a close relationship with matrices that result either from mixing of these (or some of these) blocks or from crushing of La Flexura-like basement material. For outcrops located between the proximal zone and the front, several processes are superimposed. The efficient mixing of Socompa rocks (or Socompa and basement rocks) generates matrices with chemical and isotopic compositions distinct from those of the blocks they are in contact with. The overall result of our study shows a very dynamic matrix, in which mixing is efficient right up to the top level of the avalanche. Whatever the mechanisms involved, this strong mixing was probably related to a very fluid state throughout nearly all of the avalanche, at least during certain stages of emplacement, and before the formation of granular faults. This questions the classical vision of debris

avalanches; they must be viewed as a complex flow (subject to rheological changes) rather than a granular mass spreading only along its base. The fact that the matrix of the avalanche most certainly behaved as a fluid is in agreement with long-distance transportation over a low slope observed for debris avalanches worldwide.

Our study demonstrates that only isotope geochemistry is able to quantify the matrix formation. Thus, our approach deserves other case studies in order to test conclusions drawn on the Socompa debris avalanche deposits. In order to optimize the number of isotope measurements, we believe it makes sense to focus sampling on a longitudinal profile, and possibly a transverse one where preferential stretching is observed. There, sampling of blocks and matrices at contact must be favored. Moreover, it is also appropriate to consider deposits that can be sampled over their whole thickness, from base to top, in order to better determine vertical lengths of mixing and the influence of basement rocks.

Acknowledgments

The authors wish to thank Jean-François Marini (head of IRD-Chile) and the whole IRD Santiago team (a special thanks to Nelda Leiva) for their welcome as well as logistical support during the three sampling campaigns of Socompa deposits. The help of Jean-Luc Froger, Thomas Shea, and Eder Gonzales was also greatly appreciated. The authors are grateful to Delphine Auclair for TIMS maintenance and support during Sr-Nd isotope analyses and to Mhammed Benbakkar for ICP-AES analyses. Frances van Wyk de Vries helped us with the quality of the manuscript, and Jim Vallance made helpful comments on a previous version of the manuscript. The paper was improved by critical reviews by Jeremy Richards, Allen Glazner, and Editor Cin-Ty Lee. Funding for this study was initially provided by the INSU project Reliefs de la Terre 2007/2008. This is Laboratory of Excellence ClerVolc contribution n°93.

References

Campbell, C. S. (1989), Self-lubrication for long runout landslides, *J. Geol.*, *97*, 653–665.

Capra, L., J. L. Macías, K. M. Scott, M. Abrams, and V. H. Garduño-Monroy (2002), Debris avalanches and debris flows transformed from collapses in the Trans-Mexican Volcanic Belt, Mexico—Behavior, and implications for hazard assessment, *J. Volcanol. Geotherm. Res.*, *113*, 81–110.

Chauvel, C., and J. Blichert-Toft (2001), A hafnium and trace element perspective on melting of the depleted mantle, *Earth Planet. Sci. Lett.*, *190*, 137–151.

Collins, G. S., and H. J. Melosh (2003), Acoustic fluidization and the extraordinary mobility of sturzstroms, *J. Geophys. Res.*, *108*(B10), 2473, doi:10.1029/2003JB002465.

Crandell, D. R. (1989), Gigantic debris avalanche of Pleistocene age from ancestral Mount Shasta Volcano, California, and debris-avalanche hazard zonation, *U.S. Geol. Surv. Bull. 1861*, 32 p.

Crandell, D. R., C. D. Miller, H. X. Glicken, R. L. Christiansen, and C. G. Newhall (1984), Catastrophic debris avalanche from ancestral Mount Shasta volcano, California, *Geology*, *12*, 143–146.

Davies, T. R., and M. J. McSaveney (1999), Runout of dry granular avalanches, *Can. Geotech. J.*, *3*, 313–320.

Debaille, V., R. Doucelance, P. Schiano, and D. Weis (2006), Multi-stage mixing in subduction zones: Application to Merapi volcano (Java Island, Sunda Arc), *Geochim. Cosmochim. Acta*, *70*, 723–741.

Deruelle, B. (1978), The Negros de Aras nuee ardente deposits: A cataclysmic eruption of Socompa volcano (Andes of Atacama, north Chile), *Bull. Volcanol.*, *413*, 175–186.

Francis, P. W., M. Gardeweg, C. F. Ramirez, and D. A. Rothery (1985), Catastrophic debris avalanche deposit of Socompa volcano, northern Chile, *Geology*, *13*, 600–603.

Iverson, R. M., and R. P. Denlinger (2001), Flow of variably fluidized granular masses across three-dimensional terrain: 1. Coulomb mixture theory, *J. Geophys. Res.*, *106*, 537–552.

Jacobsen, S. B., and G. J. Wasserburg (1984), Sm-Nd isotopic evolution of chondrites and achondrites, II, *Earth Planet. Sci. Lett.*, *67*, 137–150.

Kelfoun, K., and T. H. Druitt (2005), Numerical modeling of the emplacement of Socompa rock avalanche, *Chile, J. Geophys. Res.*, *110*, B12202, doi:10.1029/2005JB003758.

Kelfoun, K., T. Druitt, B. van Wyk de Vries, and M.-N. Guilbaud (2008), Topographic reflection of the Socompa debris avalanche, *Chile, Bull. Volcanol.*, *70*, 1169–1187.

Legros, F. (2002), The mobility of long-runout landslides, *Eng. Geol.*, *63*, 301–331.

Le Maître, R. W. (2002), *Igneous Rocks. A Classification and Glossary of Terms, Recommendations of the International Union of Geological Sciences Subcommission on the Systematics of Igneous Rocks*, 236 pp., Cambridge Univ. Press, Cambridge, U. K.

Mamani, M., G. Wörner, and T. Sempere (2010), Geochemical variations in igneous rocks of the Central Andean orocline (13°S to 18°S): Tracing crustal thickening and magma generation through time and space, *GSA Bull.*, *122*, 162–182.

Mangeney, A., P. Heinrich, and R. Roche (2000), Analytical solution for testing debris avalanche numerical models, *Pure Appl. Geophys.*, *157*, 1081–1096.

Mollon, G., V. Richefeu, P. Villard, and D. Daudon (2012), Numerical simulation of rock avalanches: Influence of a local dissipative contact model on the collective behavior of granular flows, *J. Geophys. Res.*, *117*, F02036, doi:10.1029/2011JF002202.

Morgan, J. K., and P. J. McGovern (2005), Discrete element simulations of gravitational volcanic deformation: 1. Deformation structures and geometries, *J. Geophys. Res.*, *110*, B05402, doi:10.1029/2004JB003252.

Nesbitt, H. W., and G. M. Young (1982), Early Proterozoic climates and plate motions inferred from major element chemistry of lutites, *Nature*, *299*, 715–717.

Otha, T., and H. Arai (2007), Statistical empirical index of chemical weathering in igneous rocks: A new tool for evaluating the degree of weathering, *Chem. Geol.*, *240*, 280–297.

Pin, C., and C. Bassin (1992), Evaluation of a strontium-specific extraction chromatographic method for isotopic analysis in geological materials, *Anal. Chim. Acta*, *269*, 249–255.

Pin, C., D. Briot, C. Bassin, and F. Poitrasson (1994), Concomitant separation of strontium and samarium-neodymium for isotopic analysis in silicate samples, based on specific extraction chromatography, *Anal. Chim. Acta*, *298*, 209–217.

Ramirez, C. F. (1988), The geology of Socompa volcano and its debris avalanche deposit, northern Chile, MSc dissertation, Open Univ., Milton Keynes, U. K.

Richards, J. P., and M. Villeneuve (2001), The Llullaillaco volcano, northwest Argentina: Construction by Pleistocene volcanism and destruction by sector collapse, *J. Volcanol. Geotherm. Res.*, *105*, 77–105.

Shea, T., and B. van Wyk de Vries (2008), Structural analysis and analogue modeling of the kinematics and dynamics of rockslide avalanches, *Geosphere*, *4*, 657–686.

Siebert, L. (1984), Large volcanic debris avalanches: Characteristics of source areas, deposits, and associated eruptions, *J. Volcanol. Geotherm. Res.*, *22*, 163–197.

Stoopes, G. R., and M. F. Sheridan (1992), Giant debris avalanches from the Colima Volcanic Complex, Mexico: Implications for long-runout landslides (>100 km) and hazard assessment, *Geology*, *20*, 299–302.

Ui, T. (1983), Volcanic dry avalanche deposits—Identification and comparison with nonvolcanic debris stream deposits, *J. Volcanol. Geotherm. Res.*, *18*, 135–150.

van Wyk de Vries, B., S. Self, P. W. Francis, and L. Keszthelyi (2001), A gravitational spreading origin for the Socompa debris avalanche, *J. Volcanol. Geotherm. Res.*, *105*, 225–247.

Voight, B., H. Glicken, R. J. Janda, and M. Douglass (1981), Catastrophic rockslide avalanche of may 18, in *The 1980 Eruptions of Mount St. Helens, Washington*, edited by P. Lipman and D. R. Mullineaux, U.S. Geol. Surv. Prof. Pap., 1250, 347–377.

Wadge, G., P. W. Francis, and C. F. Ramirez (1995), The Socompa collapse and avalanche event, *J. Volcanol. Geotherm. Res.*, *66*, 309–336.